Interim report: Fatigue assessment of case hardened components

Abstract

The aim with the project is to develop a virtual design approach for case hardened components. Until 2018-09-30 the main focus has been development of the computational model and fatigue predictions. Some fatigue testing has been made as well as design of the fatigue specimens needed to test the hardened material structure. The whole simulation approach has been used for predicting the tooth root bending strength of gear used Scania gear boxes where good predictions of the fatigue life was made. The next step is prediction of the fatigue life at running tests of a gear box.

Introduction

The aim with the project "Fatigue assessment of case hardened components" is to develop better models for predicting the fatigue strength of case hardened components with a min focus towards gears. Such a model will enable virtual dimensioning of the gear where, for instance, the effect of different heat treatment procedures can be investigated without a costly experimental campaign. This virtual dimensioning approach is shown in **Figure 1**.
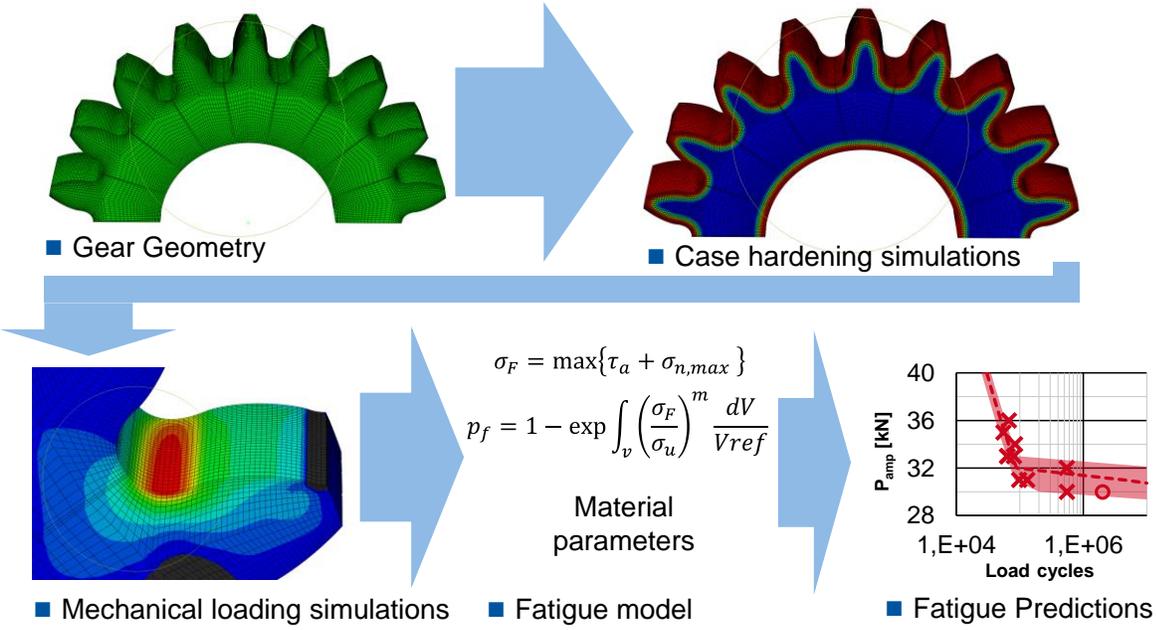

$$\sigma_F = \max\{\tau_a + \sigma_{n,max}\}$$

$$p_f = 1 - \exp \int_v \left(\frac{\sigma_F}{\sigma_u}\right)^m \frac{dV}{Vref}$$

Figure 1. Visualization of the virtual dimensioning approach developed and used in the project.

All different steps shown in **Figure 1** are developed in the project except the first "Gear geometry" which is considered as a given input.

Results during the period 2018-01-01 – 2018-09-30

During the period 2018-01-01 to 2018-09-30 the work has mostly been simulation-driven to a test machine failure in the spring 2018. Some initial testing before the test machine broke down has been made. The following steps has been are competed so far and explained in some more detail below.

- Implementation of the simulation framework in Python
- Case study of the fatigue life of gears subjected to different heat treatment
- Presentation and report at WZL Gear Conference in Aachen 2018
- Design, manufacturing and heat treatment of two types of fatigue specimens

Simulation work

During the period, the whole simulation chain has been developed using Abaqus and the programming language Python providing a simulation environment that takes a finite element mesh and results in a load life diagram based on FEM simulations of the case hardening and mechanical loading. Most time has been spent on the Weakest-link model that provides the probability of failure of the whole component based on a distribution of material properties due to case hardening.

In order exemplify the approach and show the usefulness of the developed simulation framework a case study was made to predict the fatigue life of planetary gears used by Scania. The gears where subjected to different heat treatment processes. The gears where divided into 4 different groups and then heat treated using a process with different carburization times resulting in different case hardening depths, defined as the depth from the surface where the hardness HV is HV=550 HV1. The aimed case hardening depths, denoted CHD, are 0.5 mm, 0.8 mm, 1.1 mm and 1.4 mm. The investigated gear is shown in **Figure 2**.

Figure 2. The gear used in the case study to exemplify the usefulness of the simulation framework.

Using heat treatment simulations together with the weakest-link model, accurate fatigue limit and life predictions could be made as seen in **Figure 3**. However, those results are based on a scaling of the residual stresses due to tempering and one ongoing effort is to incorporate tempering accurately in the heat treatment simulations in order to achieve correct residual stresses.
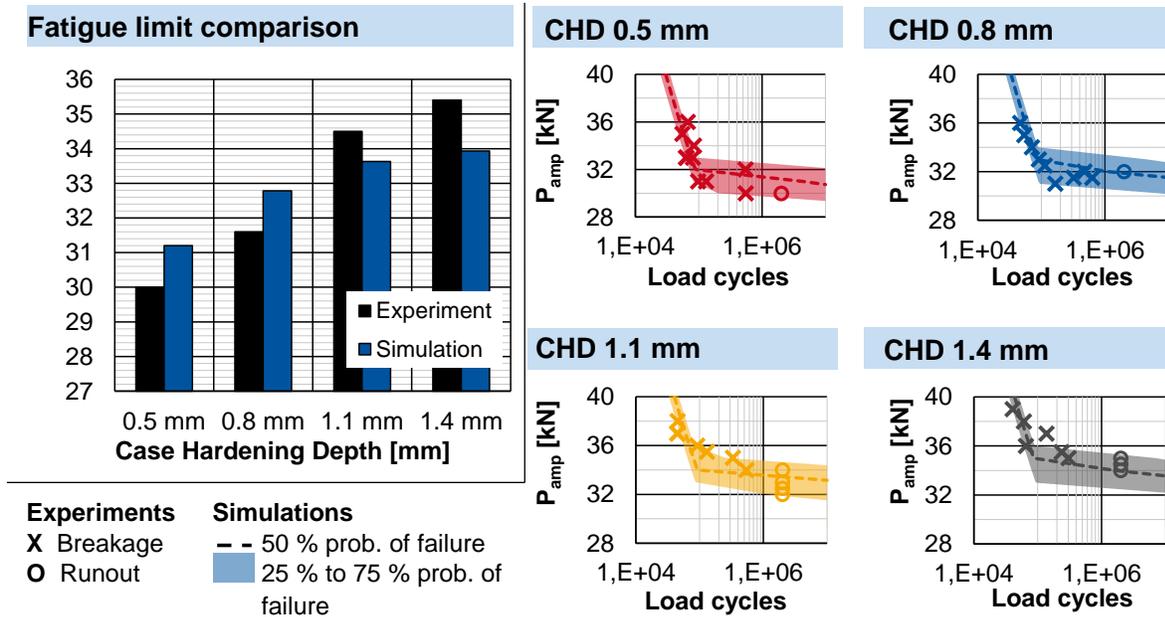

Figure 3: Fatigue limit and life predictions compared with experimental results.

The results of the case study were presented to the European gear industry at the 2018 Gear conference in Aachen, Germany and was published in the accompanying proceedings. This report is added as an appendix to this report, presenting the model and the framework in more detail.

Fatigue specimen development and testing

The plans for the fatigue specimen testing have unfortunately been severely affected by the break-down of the tension torsion test machine at the Odqvist Laboratory at KTH which lead to that the original plan of torsion testing of cylindrical specimens had to be abandoned in the project. An initial plan was that the machine could have been repaired during the summer, but inspections showed that it had to be replaced which will be done after the end of this project (during 2019). This resulted in a re-design of fatigue specimens that are tested in conventional tension compression test-machines.

Two different designs of specimens are designed that are based on bending experiments. One challenge is to achieve fatigue failure from the interior of the material is the focus of the fatigue testing is the material structure occurring under the hard case layer. The first design is a simple bending specimen that is loaded either in three- or four-point bending. This gives a good quantification of the volume effect on the fatigue limit and fatigue life. The second type of fatigue specimen is a shear bending specimen where the shear stress due to bending in the interior of the specimen is used to initiate fatigue failure. Here, a big challenge has been to make a design that has a high probability of failure from the interior but not from the surface. If the tension-torsion machine would have been in service, a direct shear test in torsion would have been possible. The different specimen designs and set-ups are shown in **Figure 3**. The difference in loaded volume in the three- and four-point bending setups is clearly visible.
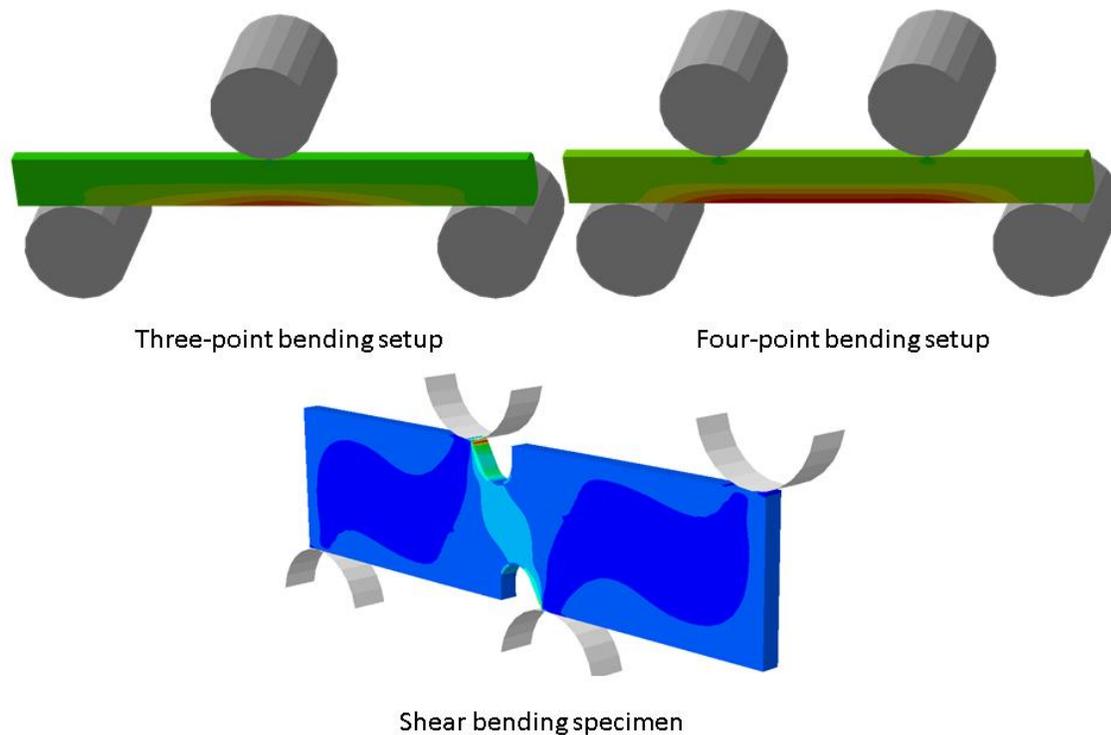
Figure 4: The two different fatigue specimen designs and the way they are tested.

The specimens are given a conventional case hardening process at Bodycote in Älvsjö, Stockholm. The three- and four-point bending testing is expected to start in the end of the autumn 2018 which is far behind schedule. This is due to the unforeseen test machine failure during the spring 2018.

Remaining work

From a modelling perspective, inclusion of tempering is deemed to be the most urgent to include in the simulations. This will remove the need of scaling the residual stresses after heat treatment simulations and thus providing more confidence in the sub-surface residual stresses that are very hard to measure. This work is ongoing and will be finished before 2018-12-31

Unfortunately, there is more remaining work regarding fatigue testing than expected, the plan was that all testing should have been performed in the end of the summer. Specimens are manufactured, and it is still very probably that the majority of the fatigue testing will e finalized before the end of the project. However, some testing will probably remain during the first 2 months of 2019 and will be reported in the final report.

The plan is to turn the appended conference report to a manuscript for submission to International Journal of Fatigue and write another manuscript with running gear box tests together with fatigue testing for submission to the same journal. The results achieved in the project will be implemented at Scania during the spring 2019.

Subject: **Predicting Gear Strength Combining Heat Treatment Simulations and Material Testing**

Author and Speaker:	Tekn. Dr. Erik Olsson
Head of Department:	Dr.-Ing. Dipl.-Wirt.-Ing. Christoph Löpenhaus
Chair Holder:	Prof. Dr.-Ing. Christian Brecher

Abstract

The trend in industry is to turn more and more into virtual product development where the whole manufacturing chain is simulated and used as input when assessing the integrity of the product. This report is a part of that development as it presents a numerical framework for predicting the fatigue limit and fatigue life of gears by simulating both the heat treatment and the mechanical loading.

The numerical framework consist of two parts. The first part is simulations of the case hardening process and of the mechanical loading. Case hardening is simulated by a combined carbon diffusion, thermal and mechanical simulation providing residual stresses, hardness values and microstructural phase fractions at every point of the component using the Finite Element (FE) method. Using the same FE-model, the mechanical loading is simulated in a second step, allowing for an easy superposition of the results.

The second part of the framework is post-processing of the results of the FE simulations for providing the probability of failure of the gear at a given load and service life. In a first step, the stresses obtained in the FE-simulations are condensed into a multiaxial effective fatigue stress for taking into account failures occurring at the whole gear tooth. This provides the local risk of fatigue in every point.

The probability of failure of the whole gear is then calculated by weakest-link theory given that if one small volume element fractures, the whole gear fractures. A recently developed weakest-link model that provides the probability of failure at a given load and at a specific number of load cycles is used. The weakest-link model is adapted to case hardened materials by defining the material parameters as function of the local hardness.

Finally, the usage of the framework is demonstrated by predicting the fatigue limit and fatigue life of a planetary gear. The fatigue predictions are compared with results from pulsator testing. Four different heat treatments are studied with different carburization times resulting in four different case hardening depths. Hardness and residual stresses are measured allowing for comparisons between experimental and simulation results throughout the simulation framework. Material data for the fatigue post-processing are taken from fatigue testing of case hardened specimens of the same material. The simulated and experimentally obtained fatigue limit and lives agree well, especially if it is taken into account that hardness and residual stresses are simulated and not obtained by measurements.

1 Introduction
Einleitung

Fatigue of case hardened materials, and especially gears, is an important but complex problem. Part of the complexity arises from the fact that the case hardening results in a graded material structure with a hard but brittle surface layer and a more soft but ductile interior. This also results in different fatigue properties depending on the distance from the surface giving different fatigue limits, mean stress sensitivities and different multiaxial fatigue be-

haviors in different parts of the material. A change in the heat treatment process or in the geometry affect these local properties and thus the fatigue life. For optimizing the heat treatment process and the geometry of the gear it is would be very beneficial to have a modelling framework that predicts the fatigue life given a gear geometry and a heat treatment process. This would reduce the amount of expensive testing iterations in product development as illustrated in **Figure 1**.
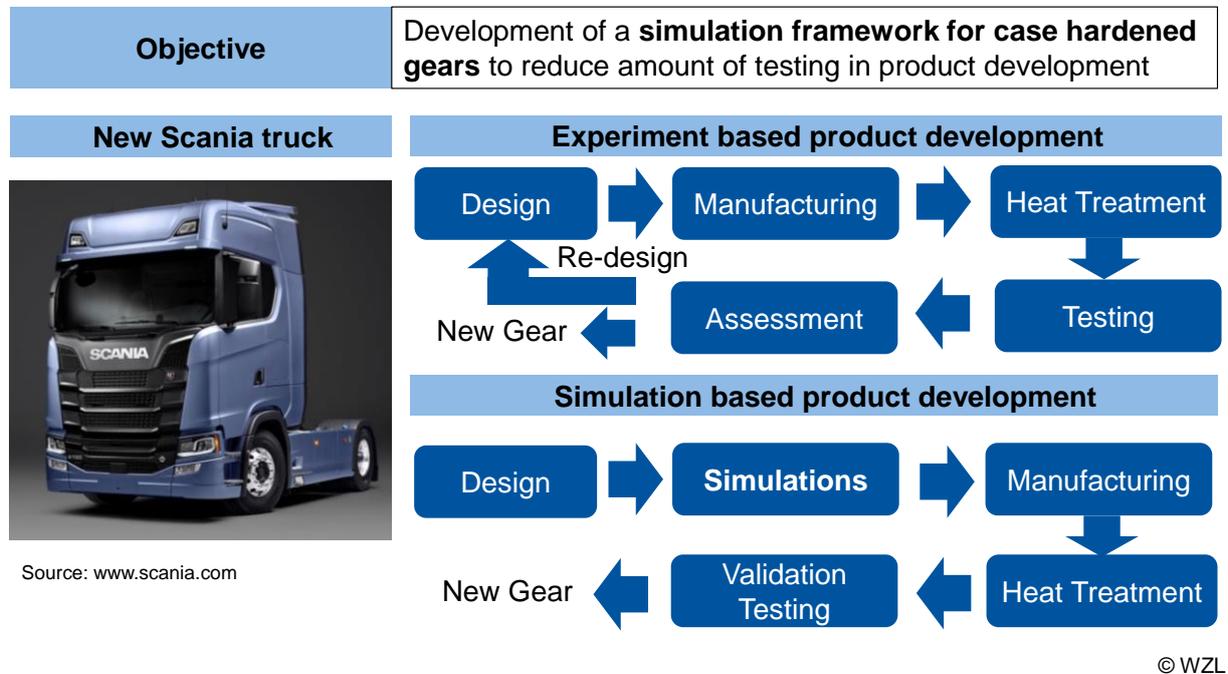

Figure 1: Motivation of the Work by Enabling a Simulation based Product Development of Case Hardened Gears.

When making changes in the heat treatment or the gear geometry, the failure mode could change. One important example is when the gear teeth are made more slender, the tensile stresses in the interior of the teeth due to the heat treatment increase. These tensile stresses together with alternating shear stresses from the contact loading could cause internal fatigue failure, a so-called Tooth Interior Fatigue Fracture (TIFF). This phenomenon was investigated by MACKALDENER AND OLSSON [MACK00, MACK01, MACK02]. Furthermore, non-fatigue related failure modes, like internal stress rupture, as described by ALBAN, caused by too large tensile stresses from the heat treatment, are also of interest to include in the framework [ALBA93]. Hence, it is important to have a modelling framework that accounts for different types of gear failures and accounts for failure in the whole gear geometry.

One complicating factor when studying fatigue failures in case hardened components is that the stress state is multiaxial with principal stress directions that change in time. Hence, for accurately being able to capture different failure modes, multiaxial fatigue criteria that reduce the time-dependent stress tensor to a scalar value, the effective fatigue stress, have to be relied upon. The scalar value is compared with a critical value which gives the *local* risk

for fatigue failure. These multiaxial fatigue criteria could, of course, be used at uniaxial loading situations as well as the effective fatigue stress takes mean stress effects into account.

It is important to consider probabilistic aspects when modelling fatigue failures, i.e. that it is only meaningful to discuss the probability that a gear will fail after a certain number of load cycles at a given load. Another probabilistic aspect is that the probability of failure is larger if the loaded volume is larger compared to a small loaded volume because the probability of finding a critical defect is higher in a larger volume. This is a particular important effect when comparing results from pulsator testing to the situation in a real gear box. In the pulsator test, only two tooth roots are loaded but in a gear box, all gear teeth roots are loaded resulting in failure at lower tooth root stresses in the gear box case [BREC16].

Volume effects could successfully be accounted for by using a modelling approach based on Weakest-Link theory giving that failure of the whole component occurs if one, small, sub-volume fails. This theory was originally formulated by WEIBULL [WEIB39]. During the recent years, the predictability capabilities of the WEIBULL weakest-link model has been critically investigated by OLSSON ET. AL [NORB07, KARL11]. A modifications of the theory, based on highly loaded regions was done by SADEK and OLSSON resulting in even better predictability for some materials [SADE14].
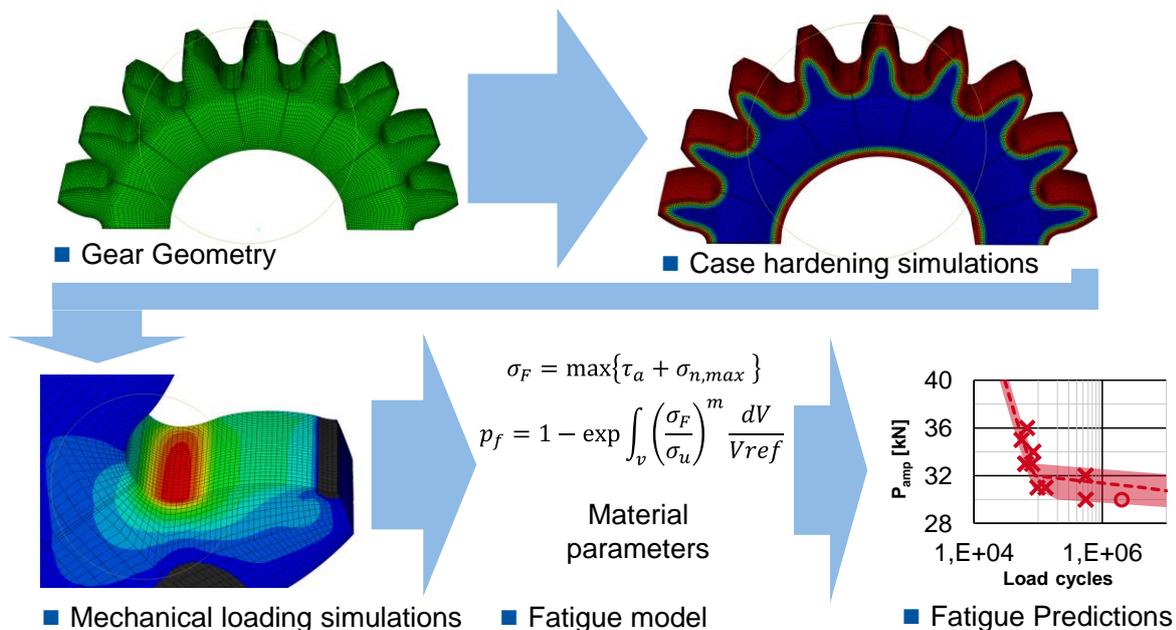
An interesting development of weakest-link models is to randomly distribute defects in the material and stating that failure will occur if a defect reaches its critical stress. One approach is to utilize the prominent work by MURAKAMI where the critical stress of an inclusion in the material is related to the size of the inclusion and the hardness of the material [MURA02]. Such a model was developed by HENSER and was successfully used for predicting the tooth root strength of beveloid gears [HENS15]. Another approach is to consider each defect as a crack and utilize Paris' law for crack propagation. If the crack grows and the stress intensity factor eventually reaches the fracture toughness of the material, the component is assumed to fracture. This approach was developed by HÄRKEGÅRD ET. AL and used by KARLÉN ET. AL for predicting the fatigue notch factor and fatigue life of notched components [FJEL08, WORM08, KARL12]. However, the crack propagation method underestimates the fatigue life due to the fact that the model does not account for the load cycles needed for fatigue crack initiation but only fatigue crack propagation. The benefit with the approaches based on defects is that they require less parameter calibration. However, this comes with the expense that information of the defect distributions has to be determined.

Both multiaxial stress states and probabilistic aspects have to be accounted for if the service life time of a gear has to be predicted based on the heat treatment. Thus, the aim with this report is to present a modelling framework that simulates heat-treatment and mechanical loading and uses information from those simulations to predict the probability of failure of gears at a given load and service life. For validation of the framework, the fatigue behaviour of a pulsator tested spur gear subjected to different heat treatments is simulated and compared with experiments.

2 Objective and Approach
Zielsetzung und Vorgehensweise

Heat treatment affects the strength of gears considerably. Current state of the art design methods for gears takes heat treatment into account by formulating the fatigue strength as function of hardness and residual stresses. However, such models cannot directly be used to investigate the effect of heat treatment parameters, like heat treatment time, temperature or carbon potential. Thus it would be beneficial to have a modelling framework that simulates the heat treatment process, given such parameters, as well as mechanical loading for predicting the strength of the gear. The aim of this report is to fill this gap by proposing a modelling framework for predicting fatigue failure of case hardened components using heat treatment simulations. A typical usage of the framework would be to answer the question if a more lengthy and thus expensive heat-treatment gives a large enough increase in fatigue strength to be worth investing in. The aim is to present an approach that works for general case hardened components but the main focus of application is gears. This modelling approach by going from gear geometry, via simulation of the heat treatment process and mechanical loading in FEM, to tooth root bending fatigue assessment is visualized in **Figure 2**.

$$\sigma_F = \max\{\tau_a + \sigma_{n,max}\}$$

$$p_f = 1 - \exp \int_v \left(\frac{\sigma_F}{\sigma_u}\right)^m \frac{dV}{Vref}$$

Material parameters

■ Gear Geometry   ■ Case hardening simulations

■ Mechanical loading simulations   ■ Fatigue model   ■ Fatigue Predictions

© WZL

Figure 2:   An Overview of the Simulation Framework Presented in this Paper

The simulation framework is based on the Finite Element Method (FEM) in order to obtain full-field information about stresses due to heat treatment and mechanical loading but also about hardness and microstructural phases. This information is utilized in state of the art fatigue post-processing models for predicting the probability of failure at given loads and at a given fatigue life. The aim with the report is both to present the needed modelling steps that are necessary for the post-processing but also to give a few examples how these steps could be implemented.

3 Simulation Framework
Simulationsrahmenprogramm

This section presents the simulation framework. The framework consists of two parts; simulations using the Finite Element Method (FEM) and post-processing of the results from the FEM. The complete framework is implemented in the finite element software Abaqus using the programming language python. In doing so, all simulations and computations, from heat treatment to fatigue assessment, are performed within the same software.

3.1 Finite Element Simulations
Finite-Elemente-Simulationen

Two types of simulations in FEM are used in this framework, simulations of the heat treatment process and simulations of the mechanical loading. The simulations are performed within the same simulation software Abaqus 6.14 and utilize the same FE discretization of the gear teeth for direct superposition of the stresses from the simulations. By doing so, there is no need for interpolating stresses between different meshes. All numerical simulations are performed using first-order elements as both the heat-treatment simulations and the mechanical contact simulations converge better with first-order elements than with higher order elements. The mesh has to be denser close the surfaces exposed to carburization in order to resolve the gradients in hardness and residual stresses.

The aim with the heat treatment simulations is to predict the hardness and the residual stresses in the gears. The simulations are performed in Abaqus by using a commercial subroutine (UMAT), called Dante. Only a segment of a gear tooth needs to be simulated with size depending of the symmetry of the gear tooth. The heat treatment simulations are performed in three sub-simulations:

- A mass diffusion simulation where the carbon is diffused into the gear material using the ambient temperature for austenitization as the temperature of the material. This is justified by the fact that the changes in temperature are much faster than the characteristic times of the carbon diffusion.
- A combined temperature and phase transformation simulation where the carbon content from the previous step is taken into account resulting in different microstructural phases depending on the changes in temperature and carbon content. Temperature changes due to phase transformations are also taken into account.
- A mechanical simulation where volume expansion of the different microstructural phases is taken into account giving residual stresses in the simulated component.

For performing those simulations steps, the following material data has to be provided:

- Carbon diffusion given as function of temperature of the steel material.
- Cooling properties of the quenching medium. This is implemented in the simulation as a film property controlling the convection on the surface as function of surface temperature.

These two functions of temperature have to be calibrated against heat treatment experiments. The phase transformations are simulated in Dante subroutine by a thermodynamic model, based on phase diagrams for steels, by utilizing the composition of the steel together with the simulated temperature changes.

From the heat-treatment simulations, the following data is obtained in each element of the finite element model which are visualized in **Figure 3**:

- Residual stresses,
- Hardness and
- Fractions of microstructural phases.

The mechanical loading is simulated by a model built-up of the discretized tooth segments used in the heat treatment simulations. This allows for including the residual stresses form the heat treatment simulations directly in the mechanical model. This combined stress state is then used for predicting the fatigue life in a post-processing step that takes the simulated hardness into account. Deformations caused by the heat treatment process could also be simulated in framework by including these deformations in the mechanical model but this is not implemented presently.
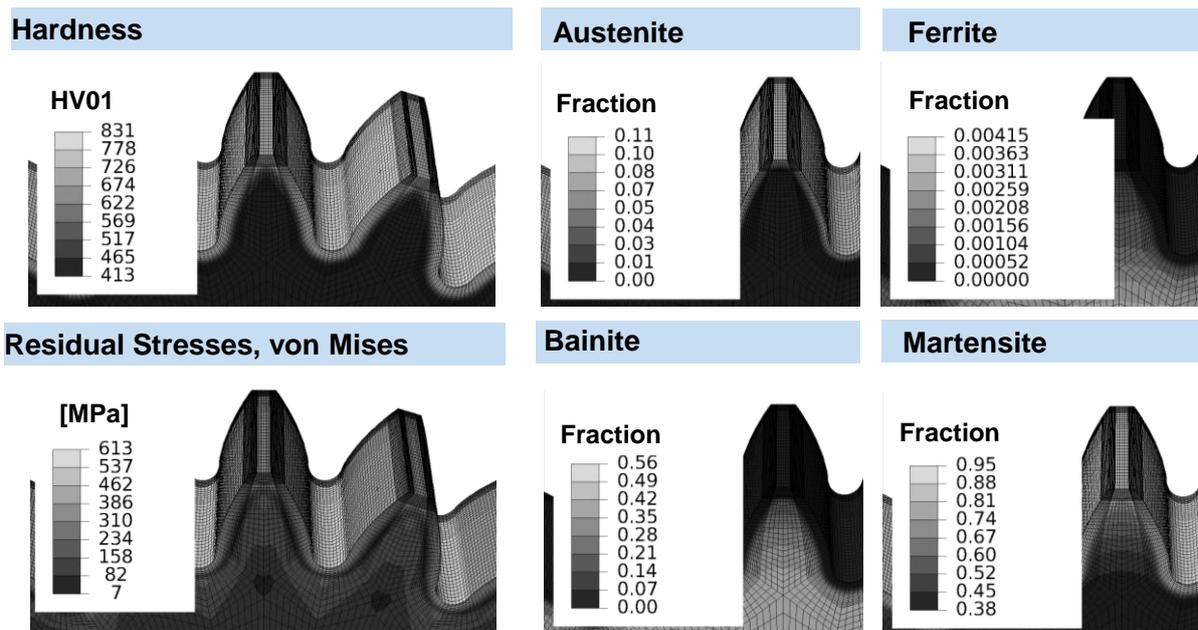
© WZL

Figure 3:   Example of a Typical Outcome from the Heat Treatment Simulations with Hardness and Residual Stresses to the Left and Fractions of Microstructural Phases to the Right.

3.2 Fatigue Post-Processing
Post-processing zur Ermüdungsberechnung

This section discusses the problem on how the probability that the gear will fracture is calculated given the stress fields obtained in the previous section. In order to do that, the time dependent stress tensor in each point has to be turned into an *effective fatigue stress*. The effective fatigue stress is then, in a second step, used for calculating the probability of failure using a weakest-link model. In both the calculation of the effective fatigue stress and in the weakest-link model, the local hardness obtained from the heat treatment simulations is taken into account.

3.2.1 Effective Fatigue Stress
Effektive Ermüdungsspannung

For each material point, the stresses are described by a time dependent stress tensor $\sigma_{ij}(t)$. To be able to compute the fatigue limit and the fatigue life, a so-called effective fatigue stress has to be used that reduces the time-dependent stress tensor to a scalar value σ_e. The simplest type of an effective fatigue stress is a largest-principle stress based effective stress where the mean stress is taken into account by a weight factor. The mean stress sensitivity can be correlated with the Vickers hardness according to WINDERLICH [WIND90].

Such a simplistic criterion does not work for multiaxial stress states and, especially so, when the principal directions changes with time. These effects can be accounted for using a multiaxial fatigue criterion. Several such criteria have been proposed in the literature. If the principal directions do not change, a criteria based on stress invariants could be used, for instance the SINES criterion or the CROSSLAND criterion [SINE59, CROS56]. Another type of criteria, which are suitable for varying principal directions, are critical plane criteria where the plane is found that maximizes a specific stress function. One widely used criterion of this type is the FINDLEY criterion which will be presented below [FIND59].

The FINDLEY criterion finds the plane where the sum of the shear stress amplitude in that plane and the maximum normal stress out of that plane, weighted with a material parameter α_F, is maximized. This criterion is stated mathematically in Equation (3-1) [FIND59].

$$\sigma_F = \left\{ \tau_a + \alpha_F \sigma_{n,max} \right\}_{max} \tag{3-1}$$

σ_F	[MPa]	Effective FINDLEY stress	α_F	[-]	FINDLEY Parameter
τ_a	[MPa]	Shear stress amplitude on the critical plane	$\sigma_{n,max}$	[MPa]	Maximum normal stress on the critical plane

The reason for focusing on the Findley criterion in this report is that this criterion in a recent investigation by BRUUN has been shown to have the best predictability when a wide range of materials is studied [BRUU15]. Furthermore, the FINDLEY parameter α_F has been shown to correlate very well with the hardness of the material and is of this reason suitable for this

type of framework were the local material properties are utilized in the same way as the WINDERLICH correlation for the mean stress sensitivity [WIND90, OLSS16]. The correlation for the FINDLEY parameter was found using data presented in the literature for a large variety of hardened steels and it was concluded that the normal stress sensitivity could accurately be described using a linear function by Equation (3-2) where the parameters take on the values $C_1 = 0.017$ and $C_2 = 8.24 \cdot 10^{-4}$ mm^2/kgf.

$$\alpha_F = C_1 + C_2 \cdot \text{HV} \tag{3-2}$$

α_F	[-]	Findley parameter	C_1	[-]	Coefficient
HV	[kgf/mm^2]	Vickers hardness, HV0.1	C_2	[mm^2/kgf]	Coefficient

It should be noted, though, that to date, there is no single effective stress criterion that works for all possible stress states and for all materials and experience and availability of material data should determine which criterion that is used. If, for instance, only tooth root strength is investigated, the simple criterion based on largest principle stress could be relied upon. However, multiaxial fatigue criteria can also be used at uniaxial conditions as their parameters will determine the mean stress effect.

The effective fatigue stress can be used in a fatigue assessment directly by comparing its maximum value to a critical value giving 50 % failure probability. However, this would neglect any influence of loaded volume and hence, it is of importance that the tested volume when determining the critical value is about the same as in the studied application.

3.2.2 Weakest-Link Modelling
Modell nach dem Weakest-Link-Ansatz

The next step in the modelling framework is to use the calculated effective fatigue stress in each material point to calculate the probability of failure of the whole component. The probabilistic modelling is based on the weakest-link theory outlined in the prominent paper by WEIBULL and is based on the following three assumptions related to the defects in the material [WEIB39]:

- Failure will occur if the strength of a sub-volume is less than the applied stress in that sub-volume.
- No interactions exist between the defects, i.e. the failure of each sub-volume is treated independently.
- Failure of the whole component occurs if failure occurs in one of the sub-volumes.

It is assumed that the probability of failure of a sub-volume is controlled by a hazard function h that is dependent on the effective fatigue stress and the number of cycles to failure. Furthermore, it is assumed that the failure probability is linearly dependent on the volume of the sub-volume dV. Thus the failure probability is given by Equation (3-3).

$$dp_f = h(\sigma_e, N) \frac{dV}{V_{ref}} \tag{3-3}$$

dp_f	[-]	Probability of failure of sub-volume dV	$h(\sigma_e, N)$	[-]	Hazard function
σ_e	[MPa]	Effective fatigue stress	N	[-]	Number of cycles to failure
dV	[mm³]	Volume of dV	V_{ref}	[mm³]	Arbitrary chosen reference volume

It is important to note that the parameters in $h(\sigma, N)$ will be dependent on the choice of the reference volume V_{ref}. Summarizing the contributions from all sub-volumes and taking the limit $dV \to 0$ gives the cumulative probability of failure as described in Equation (3-4).

$$p_f = 1 - \exp\left[-\int_V h(\sigma_e, N) \frac{dV}{V_{ref}}\right] \tag{3-4}$$

p_f	[-]	Probability of failure of the component	$h(\sigma_e, N)$	[-]	Hazard function
σ_e	[MPa]	Effective fatigue stress	N	[-]	Number of cycles to failure
dV	[mm³]	Volume of dV	V_{ref}	[mm³]	Arbitrary chosen reference volume, chosen to 1 mm² presently

The next step is to define the function $h(\sigma_e, N)$. In the original WEIBULL model, only the fatigue limit was studied, removing the dependency of the fatigue life N [WEIB39]. The hazard function $h(\sigma)$ was in that case specified according to Equation (3-5).

$$h(\sigma_e) = \left(\frac{\sigma_e}{\sigma_u}\right)^m \tag{3-5}$$

$h(\sigma_e)$	[-]	Hazard function	σ_e	[MPa]	Effective fatigue stress
σ_u	[MPa]	WEIBULL stress	m	[-]	WEIBULL exponent

This model was later extended to finite fatigue life in [OLSS16]. This was achieved using a BASQUIN relation for the WEIBULL stress σ_u above the fatigue limit and introducing a dependency of N in the WEIBULL exponent n [BASQ10]. The expression for the WEIBULL stress is defined in Equation (3-6) [WEIB39, OLSS16].

$$\sigma_u(N) = \begin{cases} \sigma_u^e \left(\dfrac{N}{N_e}\right)^{-1/b} & \text{if } N \le N_e \\ \sigma_u^e & \text{if } N \ge N_e \end{cases} \tag{3-6}$$

$\sigma_u(N)$	[MPa]	WEIBULL stress at N cycles to failure	σ_u^e	[MPa]	WEIBULL stress at the endurance limit
N_e	[-]	Load cycles at the transition between the finite fatigue limit regime	b	[-]	Fatigue life exponent

Presently, a model without a fatigue limit is proposed but with different fatigue life exponents in different regimes, creating a "knee" in a stress-life diagram. It is also reasonable to

introduce a dependency on the number of load cycles to failure in the parameter controlling the scatter, the WEIBULL exponent m, as the scatter is usually higher around the fatigue limit than at shorter fatigue live. A higher WEIBULL exponent results in lower scatter and this behavior can be accounted for in the same way as for the WEIBULL stress. The expressions for the WEIBULL stress and exponent are presented in Equations (3.7) – (3.9).

$$\sigma_u(N) = \sigma_u^k \left(\frac{N}{N_k}\right)^{-1/b} \tag{3-7}$$

$$m(N) = m_k \left(\frac{N}{N_k}\right)^{-1/b} \tag{3-8}$$

$$b = \begin{cases} b_1 & N \le N_k \\ b_2 & N > N_k \end{cases} \tag{3-9}$$

$\sigma_u(N)$	[MPa]	WEILBULL stress at N cycles to failure	σ_u^k	[MPa]	WEIBULL stress at N_k cycles
$m(N)$	[-]	WEILBULL exponent at N cycles to failure	m_k	[-]	Weibull exponent at N_k number of load cycles
b_1	[-]	Fatigue life exponent for short lives $(N \le N_k)$	N_k	[-]	Load cycles at the "knee" in the stress life diagram
b_2	[-]	Fatigue life exponent for long lives $(N > N_k)$	N	[-]	Cycles to failure

When $b_2 \to \infty$, a model with a fatigue limit is obtained, i. e. infinite fatigue life for loads below the fatigue limit.

Equations (3.4) to (3.9) present a weakest-link model for predicting the fatigue life of a component with homogenous properties which is not the case for a heat treated gear where a gradient in material properties is seen. This is accounted for by introducing a dependency on the hardness in the WEIBULL stress and in the WEIBULL exponent. It is a fact from fatigue testing that the fatigue limit is increasing by the hardness and that effect is accounted for in the present model by making the WEIBULL stress at the fatigue limit dependent on the hardness. Based on the results in OLSSON ET. AL, a linear model for σ_u is used according to by Equation (3-10) [OLSS16].

$$\sigma_u^k = A_1 + A_2 \cdot \text{HV} \tag{3-10}$$

σ_u^k	[MPa]	WEIBULL stress at the fatigue limit	A_1	[MPa]	Coefficient
HV	[kgf/ mm²]	Vickers hardness	A_2	[N/kgf]	Coefficient

It is also a fact from fatigue testing that harder materials show more scatter concerning the fatigue limit than softer materials. This was, for instance, investigated by BRÖMSEN and agrees with fatigue testing of the present material as well [BRÖM05]. This behavior is accounted for in the model by having the WEIBULL exponent at N_k number of cycles, m_k, as a function of the hardness. In BRÖMSEN, this behavior is written by Equation (3-11) [BRÖM05].

$$m_k = \frac{B}{\text{HV}^2}$$

(3-11)

m_k	[-]	WEIBULL exponent at N_k number of load cycles	B	[mm^4/kgf^2]	Coefficient
HV	[kgf/mm^2]	Vickers hardness			

In the work by BRÖMSEN, B has the value of $6.4 \cdot 10^6$ mm^4/kgf^2 but in this work B will be fitted to fatigue experiments of the present material [BRÖM05]. It could also be reasonable to introduce a dependency on the hardness into the fatigue life exponents b_1 and b_2. However, no evidence of this dependency could be found from the fatigue specimen testing and thus b_1 and b_2 are assumed to be independent on the hardness which reduces the amount of material parameters.

A final note is that an approach based on inclusions can be included in the framework by formulating the hazard function h as the probability that an inclusion of a critical size exists in the sub-volume dV. By doing so, the approach by HENSER could be used in the framework [HENS15]. The critical inclusion size will then be dependent on the local stress and the hardness according to MURAKAMI [MURA02]. However, this extension of the weakest link model will be left for future investigations.

4 Example of the Approach
Validierung des Ansatzes an einer Beispielverzahnung

In this section, an example is presented where the framework is demonstrated by predicting the fatigue limit and the fatigue life of a case hardened spur gear at pulsator testing. The effect of different case hardening depths is given a particular focus. The gear in this investigation was a planetary gear used in one type of gear boxes in trucks from the Swedish company Scania. The gear is pictured in **Figure 4** together with gear parameters according to DIN 3960:1987 [DIN87]. The gears were manufactured of a Swedish steel denoted 2506 and its chemical composition is also presented in Figure 4.

4.1 Experimental Study
Experimentelle Arbeiten

In order to investigate the effect of heat treatment on the fatigue performance of the gears and to investigate if the hardness and residual stresses can be predicted using heat treatment simulations, the gears where subjected to different heat treatment processes. The gears where divided into 4 different groups and then heat treated using a process with different carburization times resulting in different case hardening depths, defined as the depth from the surface where the hardness HV is HV = 550 HV1. The aimed case hardening depths, denoted CHD, are 0.5 mm, 0.8 mm, 1.1 mm and 1.4 mm.

Parameter	Value
Number of teeth z [-]	20
Module m_n [mm]	3.65
Pressure angle α [°]	22.5
Facewidth b [mm]	14.0
Helix angle [°]	0
Center Distance [mm]	83.5

Element	C	Si	Mn	P	S	Cr	Ni	Mo	Cu	Al	Fe
Weight %	0.23	0.2	0.97	0.01	0.033	0.6	0.36	0.7	0.16	0.27	Balance

© WZL

Figure 4: Photograph of the Gear Investigated in this Report Together with its Chemical Components and Gear Parameters According to DIN 3960:1987 [DIN87].

The heat treatment process is sketched in **Figure 5**. The initial step, where the temperature was increased from $T = 780\ °C$ to $T = 930\ °C$ at a constant carbon activity of 0.48 % C was the same for all heat treatments and occurs for $t_1 = 5800\ s$. The process times t_2, when the carbon activity is at 0.85 %, t_3, when the temperature is at $T = 930\ °C$, and t_4, the time when the gears are quenched in oil, differ for the different aimed case hardening depths and are presented in Figure 4. After quenching, the gears were tempered for a time $t_5 = 3600\ s$ for all aimed case hardening depths at a temperature of $T = 120\ °C$.

The hardness profiles and residual stresses obtained with these case hardening processes will be discussed in the next section where those results are compared with simulated values. After the heat treatments, the gear tooth flanks, but not the tooth roots, were ground. No shot peening of the gears was performed.

The gear testing has been performed at Scania and the focus of the testing was the finite-life regime. The testing started at a load corresponding to an expected failure at about 50 000 load cycles. The loading was decreased with 1 kN per test, in order to explore the finite-life regime, until a run-out was obtained. Thereafter, some additional tests were performed around the run-out load to get an estimation of the fatigue limit. Using such an approach the finite-life regime will be well explored but the estimated fatigue limit is affected with statistical uncertainties.

The load frequency was set to $f = 30\ Hz$ which is the standard procedure described in [FVA12]. The load ratio $R = P_{min}/P_{max}$ was set to $R = 0.1$ in order to not lose contact between the gear and the pulsator jaws used to apply the load. Several tests were performed on one single gear by rotating the gear a few teeth for the new test. Hence, it was assumed that the testing does only affect the two loaded teeth.

Heat treatment process
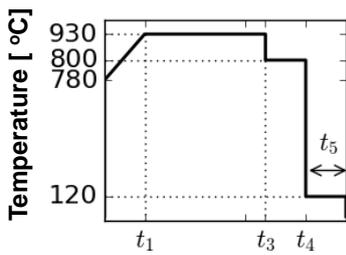
- Quenching in oil
- Tempering
  $t = 3600\ s$
  $T = 120\ ^oC$

Time steps in the case hardening process
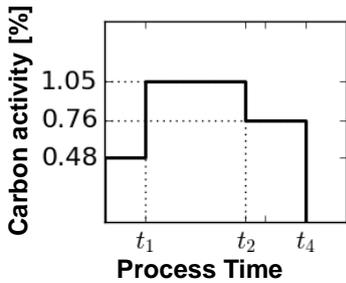
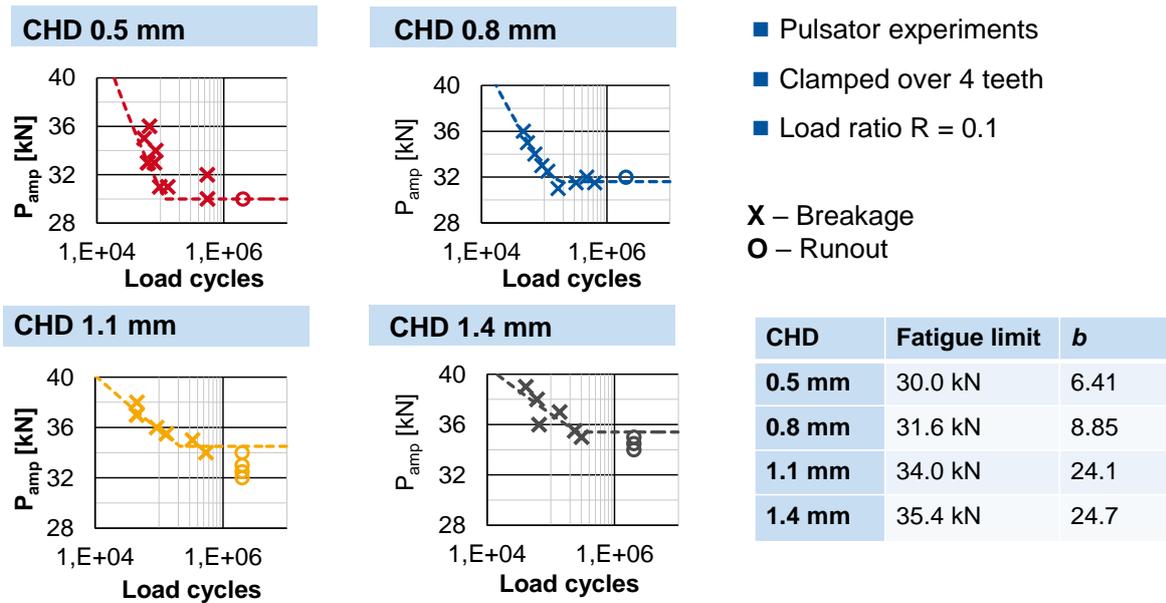| CHD	t_1 [s]	t_2 [s]	t_3 [s]	t_4 [s]	t_5 [s]
0.5 mm	5800	10300	10660	14100	3600
0.8 mm	5800	15800	17400	21500	3600
1.1 mm	5800	27700	31800	35700	3600
1.4 mm	5800	38400	46000	50400	3600

© WZL

Figure 5: Sketch of the Temperature and Carbon Activity During the Case Hardening Process.

The outcome of the fatigue testing is presented at load-life diagrams (SN-curves) with the load amplitude P_{amp} on the ordinate in **Figure 6** where two different regimes can be identified, the finite life regime and the fatigue limit regime. In the finite life regime, the BASQUIN relation is used to describe the allowed load as number of cycles to failure. In the fatigue limit regime, the gear is assumed to survive an infinite number of load cycles if the load is below the fatigue limit denoted P_e. The needed load to obtain a given fatigue life N, valid in both regimes can thus be calculated using Equation (4-1) with parameters determined using the maximum likelihood method.

$$P_{amp}(N) = \begin{cases} P_e \left(\dfrac{N}{N_e} \right)^{-1/b} & \text{if } N \leq N_e \\ P_e & \text{if } N \geq N_e \end{cases}$$

(4-1)

P_{amp}	[N]	Load amplitude	N	[-]	Load cycles to failure
P_e	[kN]	Fatigue limit load	N_e	[-]	Load cycles at the transition between the fatigue limit regime and the finite life regime.
b	[-]	Fatigue life exponent			

The determined fatigue limits and fatigue exponents are presented in Figure 6 where it is seen that the fatigue exponents increases notably with increasing case hardening depth.

CHD 0.5 mm | **CHD 0.8 mm**

■ Pulsator experiments
■ Clamped over 4 teeth
■ Load ratio R = 0.1

X – Breakage
O – Runout

CHD	Fatigue limit	b
0.5 mm	30.0 kN	6.41
0.8 mm	31.6 kN	8.85
1.1 mm	34.0 kN	24.1
1.4 mm	35.4 kN	24.7

© WZL

Figure 6: The Outcome of the Pulsator Experiments in the form of Load-Life Diagrams. There is Only one Run-out at each Load level.

4.2 Numerical Simulations
Numerische Simulationen

The heat treatment of the gears was simulated using the carburization levels and temperature presented in Figure 5 as input data. Due to symmetry only ¼ of a gear tooth needed to be modelled for simulating the heat treatment.

A comparison between the simulated and measured tooth root hardness is presented in **Figure 7** where a good agreement is found between the experimental and numerical values close to the surface. However, the discrepancies increase with the distance from the surface. This indicates that the carbon diffusivity would benefit from some further calibration against experiments. A note is that the surface hardness is approximately the same, 820 HV01 for all cases. If the fatigue crack initiates at, or close-to the surface, the increase in fatigue strength has to be caused by larger compressive residual stresses at the higher case depths as the mean stress is decreased.

The residual stresses are measured using X-ray diffraction and compared with experimental values. As the stresses are only measured down to a depth of $d = 0.16$ mm which is approximately the thickness of two elements in the meshed model, the mean of the measured stresses should be compared with the mean of the simulated stresses over the two outermost elements.

Experimental and simulated root hardness
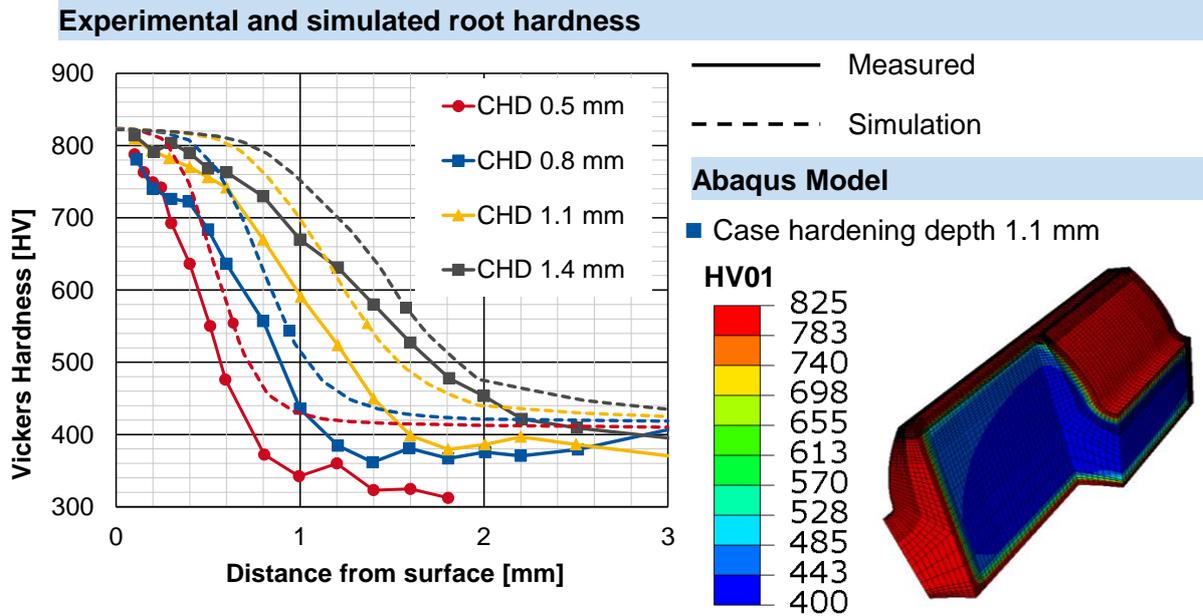
© WZL

Figure 7:   Comparison between Numerically Simulated Vickers Hardness and Experimentally Determined Values (HV1).

The measured values are presented in the top right in **Figure 8**. The measured values are similar for all case hardening depths except for CHD 0.5 mm. One explanation for this outlier could be a slower quenching for this process.
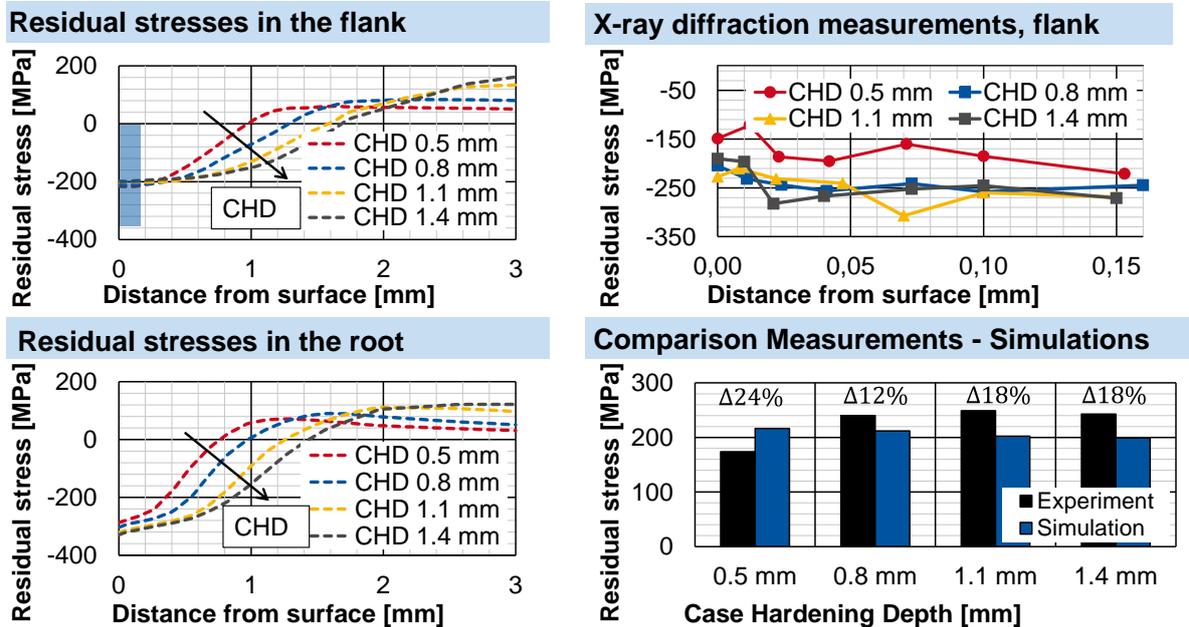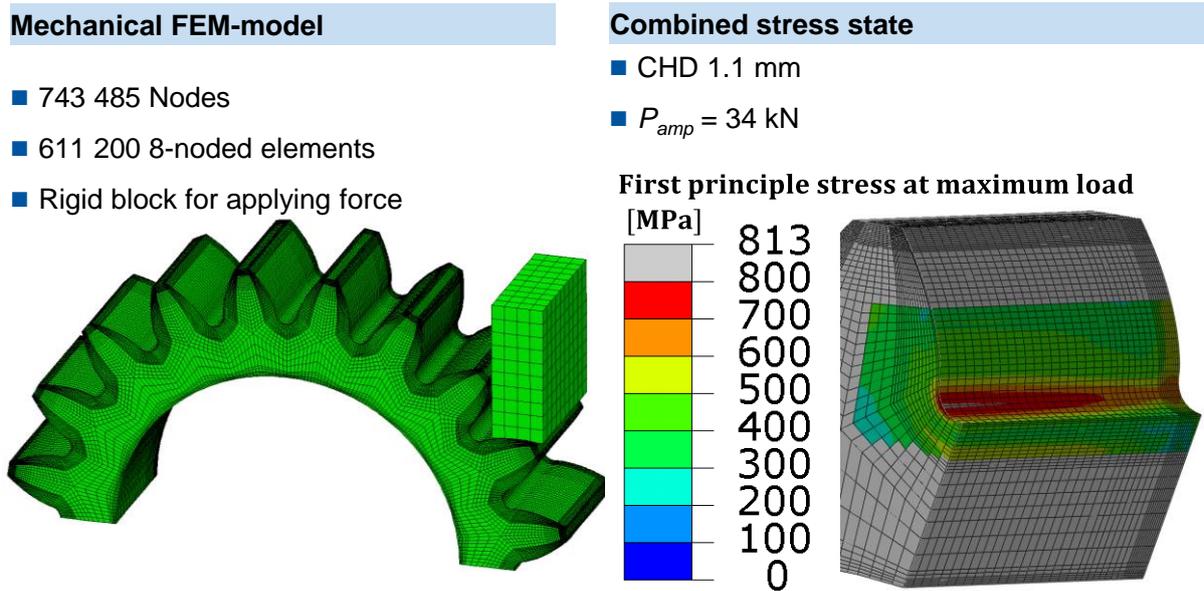

© WZL

Figure 8:   Simulated and Measured Residual Stresses. The Depth in the Tooth Flanks Investigated with X-ray Diffraction is Marked in the upper Left Figure.

The comparison between simulations and measurements is presented to the lower right in Figure 8 where discrepancies between 12 % to 24 % is seen As setpoint values are used for the heat treatment simulations and not measured temperatures and carbon activities in the heat treatment oven it is judged that an acceptable agreement is found with the measurements. Furthermore, conditions inside the oven and during quenching might vary from position to position due to different thermal masses which would affect heating and cooling rates.

For simulating the mechanical loading at the pulsator testing, one fourth of a gear needs to be modelled due to symmetry conditions. The model, when taken all symmetries into account, is shown to the left in **Figure 9** together with the rigid block used to apply the load. Only two load levels need to be analysed, the maximum and the minimum load. Pulsator loading of gear teeth is not strictly a linear problem as an increase in load moves the contact point on the tooth flank. However, by investigating different load levels in the relevant loading range, $P_{amp} = 28$ kN to 40 kN, it is concluded that this non-linearity is small and thus is not taken into account. Hence, only two FE-simulations are performed for the pulsator model one for the maximum load and one for the minimum load. For the different load levels studied, the stress fields due to mechanical loading are linearly scaled using the results from the simulated levels.

Mechanical FEM-model

- 743 485 Nodes
- 611 200 8-noded elements
- Rigid block for applying force

Combined stress state

- CHD 1.1 mm
- $P_{amp} = 34$ kN

First principle stress at maximum load

© WZL

Figure 9:   The Mechanical FEM Model with all Symmetries Taken into Account and the Resulting Largest Principal Stress of the Combined Stress State at Maximum Load.

4.3 Fatigue Predictions
Vorhersage der Ermüdungsfestigkeit

The fatigue post-processing needs several material parameters. For evaluation of the Findley stress, the aforementioned two parameters C_1 and C_2 are needed with values found in the literature [OLSS16]. The fatigue behavior of the SS2506 steel has been extensively investigated in the literature [PRES91, ALFR01, MACK01]. In an ongoing experimental study, specimens were case hardened to different case hardening depths and surface hardness and thereafter tested in tension-torsion load cycles to obtain multiaxial fatigue and weakest-link parameters and those material parameters were used in the post-processing.

It is important to emphasize that the reference volume V_{ref} is set to 1 mm^3 and the presented material parameters are only valid when using this reference volume in the simulations. Using a calibration for predicting the fatigue limit with the maximum likelihood method, A_1 and A_2 take on the values $A_1 = 140 \text{ MPa}$ and $A_2 = 0.71 \text{ N/kgf}$. The parameter controlling the scatter B was found to be $B = 11.1 \cdot 10^6 \text{ mm}^4/\text{kgf}^2$ resulting in more narrow failure distributions for the present material than for the materials investigated in [BRÖM05].

The fatigue life parameters are harder to calibrate and the calibration is performed by penalizing predictions that give experimental life outcomes that not lie between 25 % and 75 % failure probability. Using such an approach the fatigue life exponents are estimated to be around $b_1 = 5$ and $b_2 = 200$. The transition, or the "knee" between the different regimes, is determined to be about $N_k = 10^5$ load cycles.

The outcome of the weakest-link model is visualized in **Figure 10**. To the left is the prediction for the fatigue limit, here defined as a failure probability of 50 % at 2 million load cycles to be consistent with the experiments, compared with the experimental values from Figure 6. The prediction accuracy has to be considered good remembering that the case hardening simulations did not exactly match the experimentally obtained case depths and residual stress values. For the lowest case hardening depth, CHD = 0.5 mm, the predicted residual stresses were too high compared to the measured values and for the two highest case depths, the simulated residual stresses were too low. This is consistent with the fatigue limit predictions where a too high fatigue limit is predicted for CHD = 0.5 mm case hardening depth and too low predicted fatigue limits for the case depths of 1.1 mm and 1.4 mm. Furthermore, the model correctly predicts that the largest increase in fatigue limit is when the case depth is increased from 0.8 mm to 1.1 mm. It should also be remembered that the experimentally obtained fatigue limits were not determined using a standard procedure and are thus affected from statistical uncertainties.

The outcome regarding the fatigue lives is presented for the four simulated case hardening depths to the right in Figure 10 in the form of an area representing failure probabilities between 25 % and 75 %. The failure probability of 50 % is marked with a dashed line. Also here a decent agreement with the experimental values is seen with most of the outcomes falling into the range with 25 % to 75 % failure probability. It should also be remembered

that a discrepancy between experimental and simulated fatigue limit has a noticeable effect on the predicted fatigue life with a too low predicted fatigue limit leading to a significantly lower predicted fatigue life than in the experiments. This explains the discrepancy for the case hardening depth of $CHD = 1.4$ mm.
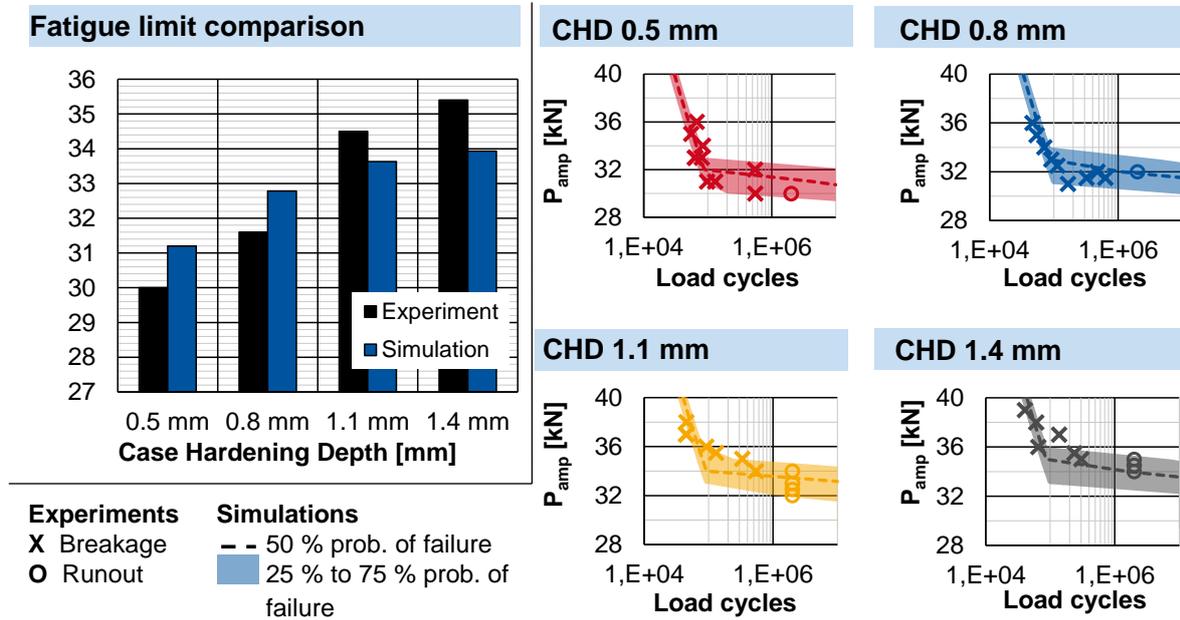
Figure 10: Comparison between Experimental and Simulated Fatigue Limits and Fatigue Lives.

5 Summary and Outlook
Zusammenfassung und Ausblick

A simulation framework for predicting the influence of the heat treatment on the fatigue behavior of case hardened gears is presented in this report. The framework consist of two parts, a finite element simulation part where the heat treatment process and mechanical loading is analyzed and a fatigue post-processing part of the finite element results. The usage of the framework has been demonstrated by predicting the change in fatigue limit and fatigue life when a spur gear is carburized for four different times. The predictions show a good agreement with results from pulsator testing, especially as the evaluation uses simulated hardness and residual stresses. The predicted residual stresses are lower than the measured values for the two heat treatments with the largest case hardening depths which results in a slightly too low predicted fatigue limit. This illustrates the importance of accurate models throughout the whole simulation framework.

The predictability of the framework is highly dependent on having reliable material models and material properties both for the case hardening simulations and the fatigue post-processing. The case hardening parameters have to be calibrated against heat treatment ex-

periments where the carbon diffusion and resulting hardness is used to obtain carbon diffusivities and cooling properties of the quenching medium.

The fatigue post-processing needs an effective stress measure and a weakest-link model that provides the probability of failure of a stressed sub-volume. Presently, the FINDLEY effective stress has been used together with a WEIBULL model for the weakest-link behavior as such a model has been used in an ongoing work for the steel studied in the experimental section. The material properties are in this case obtained by fatigue testing of case hardened specimens. Another option is to calibrate the model against experiments performed on gears and use the presented framework in reverse for determining material parameters. Nevertheless, as long as reliable material data is provided, the framework could be useful and the better knowledge about the material, the better fatigue predictions could be made using the framework.

Two extensions of the framework are planned presently. Firstly, the weakest-link approach by HENSER, where inclusions are randomly positioned in the gear, should be implemented in the framework [HENS15]. This could be implemented by formulating the argument in the weakest-link integral as the probability that an inclusion of a critical size is in the sub-volume. The critical inclusion size will then be dependent on the local hardness. A large benefit with the HENSER approach is that the number of material parameters could be reduced. The second extension is to account for the different microstructural phases in the fatigue post-processing step. In the application of the framework presented in this report, only surface or close-to surface initiated fatigue is studied where the steel has a martensitic microstructure. However, for studying fatigue initiated beneath the contact, for instance Tooth interior Fatigue Fracture (TIFF), the cracks initiate in a microstructure that contains 25 % - 75 % bainite. There are indications that bainite has a different fatigue behavior than martensite at the same hardness and thus simulated microstructural phases should be included in the fatigue post-processing for predicting TIFF [OLSS10]. Quantification of this effect is an ongoing project.

In summary, the framework presented in this report shows a promising step into virtual development in gear design. Questions in the design state like which effect a more lengthy and thus more expensive heat treatment would have on the fatigue behaviour could thus be answered without a costly experimental investigation.

Acknowledgement

6 Bibliography

Literatur

[ALBA93]   Alban L. E. :
              Systematic Analysis of Gear Failures
              In: American Society for Metals (1993)

[ALFR01]   Alfredsson, B. ; Olsson, M:
              Applying multiaxial fatigue criteria to standing contact fatigue.
              In: International Journal of Fatigue Bd. 23 (2001), Nr. 6, S. 533–548

[BASQ10]   Basquin O. H.:
              The exponential law of endurance test
              In: Proceedings of the American Society for Testing and Materials. 10
              (1910): S. 625–630

[BREC16]   Brecher, C.; Löpenhaus C.; Rüngeler M.:
              Übertragung des Schrägverzahnungspulsens auf den Laufversuch mit Hilfe
              des erweiteren Fehlstellenmodells
              In: Zahnrad- und Getriebetechnik: Eigendruck Getriebekreis Aachen (2016)

[BRUU15]   Bruun Ø. A.; Härkegård G.:
              A Comparative Study of Design Code Criteria for Prediction of the Fatigue
              Limit under in-Phase and out-of-Phase Tension–Torsion Cycles
              In: International Journal of Fatigue Bd. 73 (2015), S. 1–16

[BRÖM05]   Brömsen, O:
              Steigerung der Zahnfußtragfähigkeit von einsatzgehärteten Stirnrädern
              durch automatische Geometrieoptimierung.,
              Diss. RWTH Aachen, 2005

[CROS56]   Crossland B. :
              Effect of Large Hydrostatic Pressures on the Torsional Fatigue Strength of
              an Alloy Steel.
              In: Proceeding of the International Conference on Fatigue of Metals (1956),
              S. 138-149

[DIN87]   Norm DIN 3960 (März 1987)
             Begriffe und Bestimmungsgrößen für Stirnräder (Zylinderräder) und
             Stirnradpaare (Zylinderradpaare) mit Evolentenverzahnung

[FIND58]   Findley, W N:
             A theory for the effect of mean stress on fatigue of metals under combined
             torsion and axial load or bending, 1958

[FJEL08]   Fjeldstad, A. ; Wormsen, A. ; Härkegård, G.:
             Simulation of fatigue crack growth in components with random defects.
             In: Engineering Fracture Mechanics Bd. 75 (2008), Nr. 5, S. 1184–1203

[HAIB70]   Haibach, E:
             Modifizierte lineare Schadensakkumulations-Hypothese zur
             Berücksichtigung des Dauerfestigkeitsabfalls mit fortschreitender
             Schädigung. LBFTechnische Mitteilungen TM, 50/70, 1970

[HENS15]   Henser, J:
             Berechnung der Zahnfußtragfähigkeit von Beveloidverzahnungen.,
             Diss. RWTH Aachen, 2015

[KARL11]   Karlén, K ; Olsson, M:
             A study of the volume effect and scatter at the fatigue limit – experiments
             and computations for a new specimen with separated notches.
             In: International Journal of Fatigue Bd. 33 (2011), Nr. 3, S. 363–371

[KARL12]   Karlén, K ; Olsson, M ; Ahmadi, H ; Härkegård, G :
             On the effect of random defects on the fatigue notch factor at different
             stress ratios.
             In: International Journal of Fatigue Bd. 41 (2012), S. 179–187

[MACK00]   Mackaldener, M. ; Olsson, M.:
             Interior fatigue fracture of gear teeth.
             In: Fatigue and Fracture of Engineering Materials and Structures Bd. 23,
             Blackwell Science Ltd (2000), Nr. 4, S. 283–292 — ISBN 8756-758X

[MACK01]   MackAldener, M. ; Olsson, M.:
             Tooth Interior Fatigue Fracture — computational and material aspects.
             In: International Journal of Fatigue Bd. 23 (2001), Nr. 4, S. 329–340

[MACK02]   MackAldener, M. ; Olsson, M.:
             Analysis of crack propagation during tooth interior fatigue fracture.
             In: Engineering Fracture Mechanics Bd. 69 (2002), Nr. 18, S. 2147–2162

[MURA02]   Murakami, Y.:
            Metal fatigue
            Elsevier Verlag, 2002

[NORB07]   Norberg, S. ; Olsson, M.:
            The effect of loaded volume and stress gradient on the fatigue limit.
            In: International Journal of Fatigue Bd. 29 (2007), Nr. 12, S. 2259–2272

[OLSS10]   Olsson E.
            Fatigue from artificial defects and inclusions in SKF bearing steels
            Master thesis report. KTH Royal Institute of Technology (2010)

[OLSS16]   Olsson, E. ; Olander, A. ; Öberg, M.:
            Fatigue of gears in the finite life regime — Experiments and probabilistic
            modelling.
            In: Engineering Failure Analysis Bd. 62 (2016), S. 276–286

[PRES91]   Preston, S.:
            Bending fatigue strength of carburising steel SS 2506.
            In: Materials Science and Technology Bd. 7 (1991), Nr. 2, S. 105–110

[SADE14]   Sadek, S ; Olsson, M:
            New models for prediction of high cycle fatigue failure based on highly
            loaded regions.
            In: International Journal of Fatigue Bd. 66 (2014), S. 101–110

[SINE59]   Sines. G :
            Behavior of Metals Under Complex Static and Alternating Stresses.
            In: Metal Fatigue (1st ed.) (1959), S. 145-169

[WEIB39]   Weibull, W:
            A statistical theory of the strength of materials.
            In: Ingenjörsvetenskaps Akademins Handlingar Bd. 151 (1939)

[WIND90]   Winderlich, B.:
            Das Konzept der lokalen Dauerfestigkeit und seine Anwendung auf marten-
            sitische Randschichten, insbesondere Laserhärtungschicten.
            In: Materialwissenschaften und Werkstofftechnik 21 (1990), S. 378-389

[WORM08]   Wormsen, A. ; Fjeldstad, A. ; Härkegård, G.:
            A post-processor for fatigue crack growth analysis based on a finite element
            stress field.
            In: Computer Methods in Applied Mechanics and Engineering Bd. 197
            (2008), Nr. 6, S. 834–845